

Article

# Adaptive Pitch Control of Variable-Pitch PMSG Based Wind Turbine

Jian Chen <sup>1</sup>, Bo Yang <sup>2,\*</sup>, Wenyong Duan <sup>1</sup> , Hongchun Shu <sup>2</sup>, Na An <sup>2</sup>, Libing Chen <sup>1</sup> and Tao Yu <sup>3</sup> 

<sup>1</sup> School of Electrical Engineering, Yancheng Institute of Technology, Yancheng 224051, China; cjycit@163.com (J.C.); dwy1985@126.com (W.D.); cumtclb@126.com (L.C.)

<sup>2</sup> Faculty of Electric Power Engineering, Kunming University of Science and Technology, Kunming 650500, China; yangboffg@sina.com (H.S.); Anna073000@163.com (N.A.)

<sup>3</sup> College of Electric Power, South China University of Technology, Guangzhou 510640, China; taoyu1@scut.edu.cn

\* Correspondence: yangbo\_ac@outlook.com; Tel.: +86-18314596103

Received: 29 August 2019; Accepted: 24 September 2019; Published: 1 October 2019



**Abstract:** This paper presents an adaptive pitch-angle control approach for a permanent magnet-synchronous generator-based wind turbine (PMSG-WT) connecting with a power grid to limit extracted power above the rated wind speed. In the proposed control approach, a designed perturbation observer is employed for estimating and compensating unknown parameter uncertainties, system nonlinearities, and unknown disturbances. The proposed control approach does not require full state measurements or the accurate system model. Simulation tests verify the effectiveness of the proposed control approach. The simulation results demonstrate that compared with the feedback linearizing controller, conventional vector controller with proportional-integral (PI) loops, and PI controller with gain scheduling, the proposed control approach can always maintain the extracted wind power around rated power, and has higher performance and robustness against disturbance and parameter uncertainties.

**Keywords:** pitch control; permanent magnet-synchronous generator (PMSG); limit extracted power; nonlinear adaptive control (NAC); perturbation observer

## 1. Introduction

Wind power generation systems (WPGSs) have become competitive and attractive as exhaustless and clean power sources [1–6]. According to the objectives of variable speed variable-pitch wind turbines (WT), three main operating regions can be observed [7], as illustrated in Figure 1. In Region 1, wind speed is lower than cut-in wind speed ( $V_{ci}$ ), and the WT does not operate; in Region 2, wind speed is between cut-in wind speed ( $V_{cut-in}$ ) and rated wind speed ( $V_{rated}$ ), and the maximum wind power is required to be extracted by rotor speed control; in Region 3, wind speed is between rated wind speed ( $V_{rated}$ ) and cut-out wind speed ( $V_{cut-out}$ ), and its main control objective is maintaining extracted wind power around rated power via blade pitch control and electromagnetic torque control.

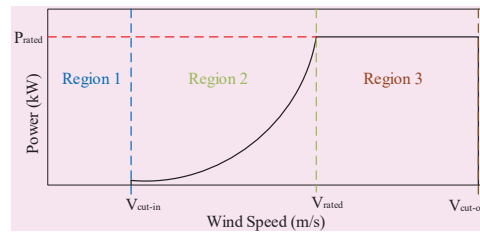


**Figure 1.** Main operating regions of the wind turbine.

To keep the wind turbine (WT) within its design limits in Region 3, blade pitch and electromagnetic torque control is primarily applied in limiting the extracted wind power [8]. As the electromagnetic torque has much faster response than the mechanical torque, the decoupled control between the WT and generator can be applied [9]. When wind speed is above rated wind speed, for the WT, the control of the mechanical rotation speed is applied to achieve the required pitch angle. The extracted wind power will vary only in proportion to mechanical rotation speed when the mechanical torque keeps at its rated value. Therefore, extracted wind power regulation is entirely dependent upon mechanical rotation speed regulation. A good tracking of a power reference can be achieved while keeping the rotor speed close to its nominal value. The variable of rotor speed reaches large values that can damage the wind turbine behavior performance in rotor speed regulation by pitch controller [10,11]. For the generator, the electromagnetic torque is required to be maintained at its rated value. When the electromagnetic torque or q-axis stator current and mechanical rotation speed are well regulated, the rated mechanical torque can be achieved. Numerous studies have used the linear techniques and designed controllers based on an approximated linear model for pitch-angle control, such as the linear quadratic Gaussian [12], conventional vector control with proportional-integral (PI) loops [13,14] and PI controller with gain scheduling (GSPI) [10,15]. As the WT contains aerodynamic nonlinearities, the linear controllers designed based on a specific operation point cannot obtain satisfactory performance under time-varying wind speed.

To enhance the performance of the conventional VC and LQG, a nonlinear controller is necessary to be designed for the WT pitch control. One effective solution is employing the feedback linearizing control (FLC) approach. The FLC has been widely and successfully applied in solving many practical nonlinear problems [8,16–18]. Compared to the controllers using linear technique and approximated linear model, a better dynamic performance of nonlinear systems can be achieved under the FLC [19]. The FLC provides fully decoupled control of the original nonlinear system and optimal performance for time-varying operation points. In reference work literature [8], an FLC with an Extended Kalman Filter has been successfully applied in the WT control. In the FLC design, full state information is required to be known. Although the FLC provides better performance than the linear quadratic regulator at low wind speeds, no enhanced performance is achieved at high wind speed, because of model uncertainties. The accurate system model is required to be known in the FLC design [20]. To make up these drawbacks of the FLC, robust control [21–23], fuzzy logic control [10,24,25], sliding mode control [26,27], and neural network control [28], have been proposed. Recently, control methods based on observers have been successfully used to reinforce the robustness of disturbances and model uncertainties in power system [29], permanent magnet-synchronous motor [30,31], photovoltaics inverters [32] and WT [33].

In this paper, a nonlinear adaptive controller (NAC) based on observers is investigated for permanent magnet-synchronous generator-based WT (PMSG-WT) to limit the extracted wind power and provide high performance in Region 3. In the designed NAC, it contains one rotor speed controller and two stator current controllers. One third-order states and perturbation observer (SPO), and two second-order perturbation observers (POs) are employed for the estimations of perturbation terms, including parameter uncertainties, coupling nonlinear dynamics, and disturbances of the PMSG-WT. The estimated perturbations are used for compensating the real perturbation and obtaining adaptive linearizing control of the PMSG-WT. The comparisons of simulation studies among the proposed NAC,

FLC, VC and GSPI under three different scenarios, e.g., ramp wind speed, random wind speed and field flux variation, are carried out to verify the effectiveness of the proposed NAC.

The remaining parts of this paper is organized as follows. The model of the PMSG-WT is presented in Section 2. Section 3 presents the design of the NAC. In Section 4, simulation studies are carried out for verifying the effectiveness of the proposed NAC in comparing with the FLC, VC and GSPI. Finally, conclusions of this work are presented in Section 5.

## 2. Model and Problem Formulation

### 2.1. PMSG-WT Configuration

In Figure 2, a gearless WPGS equipped with a PMSG is connected to the power grid through full-rate back-to-back voltage source converters. Wind power extracted by the WT is transmitted to the direct-driven PMSG. Then, the mechanical power is converted to electrical power by the PMSG. Then, the electrical power is supplied to the power grid via a machine-side converter (MSC) and a grid-side inverter (GSC). The main objective of the MSC is to extract power from wind by controlling the mechanical rotation speed and electromagnetic torque or q-axis stator current, and produce the required stator voltage, whereas the GSC has to enable decoupled control the active and reactive power required by grid codes. The operation control of these two converters can be decoupled by a DC voltage link [16].

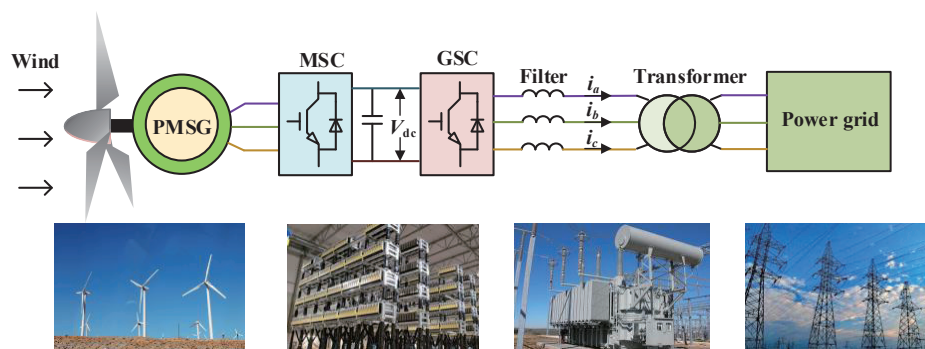


Figure 2. Configuration of a PMSG-WT.

### 2.2. Aerodynamic Model

The wind power extracted by a WT is represented as [34,35]

$$P_w = \frac{1}{2} \rho \pi R^2 V^3 C_p(\beta, \lambda) \tag{1}$$

$$\lambda = \frac{R \omega_m}{V} \tag{2}$$

where  $\beta$  is the pitch angle,  $\rho$  is the air density,  $V$  is the wind speed,  $R$  is the radius of WT,  $C_p$  is the power coefficient,  $\lambda$  is the tip speed ratio, and  $\omega_m$  is the mechanical rotation speed. The  $C_p$  can be defined as a function of  $\beta$  and  $\lambda$

$$C_p = 0.22 \left( \frac{116}{\lambda_i} - 0.4\beta - 5 \right) e^{\frac{-12.5}{\lambda_i}} \tag{3}$$

$$\frac{1}{\lambda_i} = \frac{1}{\lambda + 0.08\beta} - \frac{0.035}{\beta^3 + 1} \tag{4}$$

A hydraulic/mechanical actuator can vary the blade pitch. The following first order linear model represents a simplified model of the dynamics:

$$\dot{\beta} = -\frac{\beta}{\tau_\beta} + \frac{\beta_r}{\tau_\beta} \tag{5}$$

where  $\beta_r$  is required pitch angle, and  $\tau_\beta$  is the actuator time constant.

The state-space model of the PMSG-WT is given as [35]:

$$\dot{x} = f(x) + g_1(x)u_1 + g_2(x)u_2 + g_3(x)u_3 \tag{6}$$

where

$$\begin{aligned} f(x) &= \begin{bmatrix} -\frac{\beta}{\tau_\beta} \\ -\frac{R_s}{L_{md}}i_{md} + \frac{\omega_e L_{mq}}{L_{md}}i_{mq} \\ -\frac{R_s}{L_{mq}}i_{mq} - \frac{1}{L_{mq}}\omega_e(L_{md}i_{md} + K_e) \\ \frac{1}{J_{tot}}(T_e - T_m - T_f - B\omega_m) \end{bmatrix}, \\ g_1(x) &= [-\frac{\beta}{\tau_\beta} \ 0 \ 0 \ 0]^T, \\ g_2(x) &= [0 \ \frac{1}{L_{md}} \ 0 \ 0]^T, \\ g_3(x) &= [0 \ 0 \ \frac{1}{L_{mq}} \ 0]^T, \\ x &= [\beta \ i_{md} \ i_{mq} \ \omega_m]^T, \\ u &= [u_1, u_2, u_3]^T = [\beta_r, V_{md}, V_{mq}]^T, \\ y &= [y_1, y_2, y_3]^T = [h_1(x), h_2(x), h_3(x)]^T = [\omega_m, i_{md}, i_{mq}]^T \end{aligned}$$

where  $x \in R^4$ ,  $u \in R^3$  and  $y \in R^3$  are state vector, input vector and output vector, respectively;  $f(x)$ ,  $g(x)$  and  $h(x)$  are smooth vector fields.  $V_{md}$  and  $V_{mq}$  are the d, q axis stator voltages,  $i_{md}$  and  $i_{mq}$  are the d, q axis stator currents,  $L_{md}$  and  $L_{mq}$  are d, q axis stator inductances,  $R_s$  is the stator resistance,  $p$  is the number of pole pairs,  $K_e$  is the field flux given by the magnet,  $J_{tot}$  is the total inertia of the drive train,  $B$  is the friction coefficient of the PMSG,  $\omega_e (= p\omega_m)$  is the electrical generator rotation speed, and  $T_m$ ,  $T_f$  and  $T_e$  are the WT mechanical torque, static friction torque and electromagnetic torque, respectively.

The electromagnetic torque is expressed as:

$$T_e = p[(L_{md} - L_{mq})i_{md}i_{mq} + i_{mq}K_e] \tag{7}$$

### 2.3. Pitch Control

To maintain the extracted wind power at rated power in Region 3, it requires that the corresponding pitch angle should be achieved, which in turn requires both the mechanical rotation speed  $\omega_m$  and the mechanical torque  $T_m$  should be kept at their rated values, respectively. The rated mechanical torque  $T_{mr}$  is achieved when the electromagnetic torque  $T_e$  can track its rated value  $T_{er}$  and the  $\omega_m$  is kept at its rated value. According to Equation (7), the electromagnetic torque  $T_e$  can be maintained at  $T_{er}$  if the q-axis stator current  $i_{mq}$  can track its rated value  $i_{mqr}$  and  $i_{md}$  is kept at 0.

The brief overall control approach is shown in Figure 3. The control approach consists three controllers: two stator current controllers and a rotation speed controller.

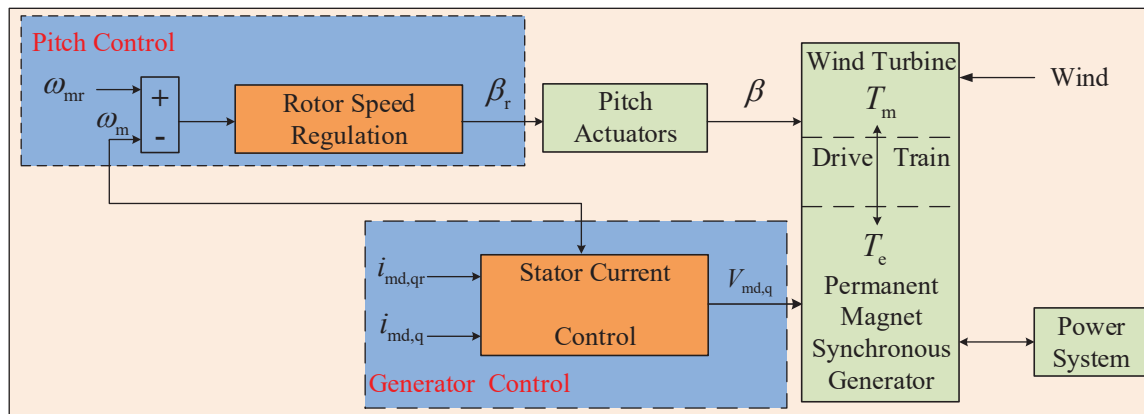


Figure 3. Brief overall control structure of the PMSG-WT.

### 3. Perturbation Observer-Based Nonlinear Adaptive Controller Design

In this section, the design of NAC for the PMSG-WT based on the feedback linearization will be presented. The NAC based on perturbation estimation proposed in [29] will be used. First, a nonlinear system is transformed as interacted subsystems through input/output linearization. Secondly, in each subsystem, uncertainties, nonlinearities and interaction among subsystems are contained in a defined perturbation term. The perturbation term is estimated via a designed observer. The estimated perturbation is used for compensating the real perturbation and obtaining adaptive linearizing control of the original nonlinear system.

#### 3.1. NAC Design of WT

##### 3.1.1. Input/Output Linearization

Input/output linearization of WT speed dynamics in system Equation (6) can be represented as

$$y_1^{(2)} = \frac{1}{J_{tot}}(\dot{T}_m - \dot{T}_e) \tag{8}$$

As the electromagnetic torque has much faster response than the mechanical torque, from the perspective of control of WT,  $\dot{T}_e \simeq 0$ . Equation (8) can be expressed as

$$\begin{aligned} y_1^{(2)} &= \frac{1}{J_{tot}}\dot{T}_m \\ &= F_1(x) + B1(x)u_1 \end{aligned} \tag{9}$$

where

$$\begin{aligned} F_1(x) &= A\left[-\frac{C_p}{\omega_m} - \frac{RV}{F^2}E\right]\frac{d\omega_m}{dt} \\ &\quad - \frac{AE\beta}{\tau_\beta}\left[-0.088e^{-12.5\tau} - \frac{0.08V^2}{F} + \frac{0.105\beta^2}{(1+\beta^3)^2}\right]\frac{d\beta}{dt} \end{aligned} \tag{10}$$

$$B1(x) = \frac{AE\beta}{\tau_\beta}\left[-0.088e^{-12.5\tau} - \frac{0.08V^2}{F} + \frac{0.105\beta^2}{(1+\beta^3)^2}\right] \tag{11}$$

where

$$\begin{aligned} A &= \frac{\rho\pi R^2 V^3}{2\omega_m} \\ E &= (39.27 - 319\tau + 1.1\beta)e^{-12.5\tau} \\ F &= \omega_m R + 0.08\beta V \\ \tau &= \frac{1}{\lambda + 0.08\beta} - \frac{0.035}{\beta^3 + 1} \end{aligned} \tag{12}$$

Please note that  $\frac{dV}{dt}$  is not included in the FLC design, which cannot be directly measured.

As  $\det[B1(x)] = \frac{AE\beta}{\tau_\beta} [-0.088e^{-12.5\tau} - \frac{0.08V^2}{F} + \frac{0.105\beta^2}{(1 + \beta^3)^2}] \neq 0$  when  $V \neq 0$  and  $\beta \neq 0$ , i.e.,  $B1(x)$  is nonsingular for all nominal operation points. Therefore, the FLC is expressed as

$$u_1 = B1(x)^{-1}(-F_1(x) + v_1) \tag{13}$$

And the nonlinear system is linearized as

$$y_1^{(2)} = v_1 \tag{14}$$

$$v_1 = \ddot{y}_{1r} + k_{11}\dot{e}_1 + k_{12}e_1 \tag{15}$$

where  $v_1$  is input of linear systems,  $k_{11}$  and  $k_{12}$  are gains of linear controller,  $y_{1r}$  is the output reference, and  $e_1 = y_{1r} - y_1$  as tracking error. The error dynamic is

$$\ddot{e}_1 + k_{11}\dot{e}_1 + k_{12}e_1 = 0 \tag{16}$$

### 3.1.2. Definition of Perturbation and State

For this subsystem, a perturbation term including all subsystem uncertainties, nonlinearities and interactions among subsystems is defined.

Define perturbation term  $\Psi_1(x)$  as:

$$S_1 : \begin{cases} \Psi_1(x) = F_1(x) + (B1(x) - B1(0))u_1 \\ B1(0) = \frac{AE\beta}{\tau_\beta} [-0.088e^{-12.5\tau} - \frac{0.08V^2}{F} + \frac{0.105\beta^2}{(1 + \beta^3)^2}] \end{cases} \tag{17}$$

where  $B1(0)$  is nominal value of  $B1(x)$ .

Defining the state vectors as  $z_{11} = y_1, z_{12} = \dot{y}_1^{(1)}, z_{13} = \Psi_1$ , and control variable as  $u_1 = \beta_r$ . The dynamic equation of the subsystem  $S_1$  becomes as

$$S_1 : \begin{cases} \dot{z}_{11} = z_{12} \\ \dot{z}_{12} = \Psi_1(x) + B1(0)u_1 \\ \dot{z}_{13} = \dot{\Psi}_1(x) \end{cases} \tag{18}$$

For subsystem  $S_1$ , several types of perturbation observers, e.g., linear Luenberger observer, sliding mode observer and high-gain observer, have been proposed [19,29,36]. High-gain observers proposed in [29] are used to estimate states and perturbations in this paper.

### 3.1.3. Design of States and Perturbation Observer

When the system output  $y_1$  is available, a third-order SPO is employed for estimations of states and perturbation of the subsystem, which is designed as

$$S1 : \begin{cases} \dot{\hat{z}}_{11} &= \hat{z}_{12} + l_{11}(z_{11} - \hat{z}_{11}) \\ \dot{\hat{z}}_{12} &= \hat{z}_{13} + l_{12}(z_{11} - \hat{z}_{11}) + B1(0)u_1 \\ \dot{\hat{z}}_{13} &= l_{13}(z_{11} - \hat{z}_{11}), \end{cases} \quad (19)$$

where  $\hat{z}_{11}$ ,  $\hat{z}_{12}$  and  $\hat{z}_{13}$  are the estimations of  $z_{11}$ ,  $z_{12}$  and  $z_{13}$ , respectively, and  $l_{11}$ ,  $l_{12}$  and  $l_{13}$  are gains of the observers, which are designed as

$$l_{ij} = \frac{\alpha_{ij}}{\epsilon_i^j} \quad (20)$$

where  $i = 1, 2, 3; j = 1, \dots, r_i + 1$ ,  $\epsilon_i$  is a scalar chosen to be within (0,1) for representing times of the time-dynamics between the real system and the observer, and parameters  $\alpha_{ij}$  are chosen so that the roots of

$$s^{r_i+1} + \alpha_{i1}s^{r_i} + \dots + \alpha_{ir_i}s + \alpha_{i(r_i+1)} = 0 \quad (21)$$

are in the open left-half complex plane.

### 3.1.4. Design of Nonlinear Adaptive Controller

The estimated perturbation is used for compensating the real perturbation, and control laws of subsystem  $S_1$  can be obtained as follows:

$$u_1 = B1(0)^{-1}(-\hat{z}_{13} + v_1) \quad (22)$$

where  $v_1$  is defined as

$$v_1 = \ddot{z}_{11r} + k_{12}(z_{11r} - \hat{z}_{11}) + k_{11}(\dot{z}_{11r} - \hat{z}_{12}) \quad (23)$$

## 3.2. NAC Design of PMSG

### 3.2.1. Input/Output Linearization

Input/output linearization of Equation (6) is represented as

$$\begin{bmatrix} y_2^{(1)} \\ y_3^{(1)} \end{bmatrix} = \begin{bmatrix} F_2(x) \\ F_3(x) \end{bmatrix} + B2(x) \begin{bmatrix} u_2 \\ u_3 \end{bmatrix} \quad (24)$$

where

$$F_2(x) = \frac{1}{L_{md}}(-i_{md}R_s + \omega_e L_{mq}i_{mq}) \quad (25)$$

$$F_3(x) = -\frac{R_s}{L_{mq}}i_{mq} - \frac{1}{L_{mq}}\omega_e(L_{md}i_{md} + K_e) \quad (26)$$

$$(27)$$

$$B2(x) = \begin{bmatrix} B_2(x) \\ B_3(x) \end{bmatrix} = \begin{bmatrix} \frac{1}{L_{md}} & 0 \\ 0 & \frac{1}{L_{mq}} \end{bmatrix} \quad (28)$$

As  $\det[B2(x)] = \frac{1}{L_{md}L_{mq}} \neq 0$ , i.e.,  $B(x)$  is nonsingular for all nominal operation points. Therefore, the FLC controller is represented as

$$\begin{pmatrix} u_2 \\ u_3 \end{pmatrix} = B_2(x)^{-1} \begin{pmatrix} -F_2(x) + v_2 \\ -F_3(x) + v_3 \end{pmatrix} \tag{29}$$

$$B_2(x)^{-1} = \begin{bmatrix} L_{md} & 0 \\ 0 & L_{mq} \end{bmatrix} \tag{30}$$

And the nonlinear system is linearized as

$$\begin{bmatrix} y_2^{(1)} \\ y_3^{(1)} \end{bmatrix} = \begin{bmatrix} v_2 \\ v_3 \end{bmatrix} \tag{31}$$

where

$$v_2 = \dot{y}_{2r} + k_{21}e_2 \tag{32}$$

$$v_3 = \dot{y}_{3r} + k_{31}e_3 \tag{33}$$

where  $v_2$  and  $v_3$  are inputs of linear systems,  $k_{21}$  and  $k_{31}$  are gains of linear controller,  $y_{2r}$  and  $y_{3r}$  the output references. Define  $e_2 = y_{2r} - y_2$  and  $e_3 = y_{3r} - y_3$  as tracking errors, the error dynamics are

$$\dot{e}_2 + k_{21}e_2 = 0 \tag{34}$$

$$\dot{e}_3 + k_{31}e_3 = 0 \tag{35}$$

### 3.2.2. Definition of Perturbation and State

Define perturbation terms  $\Psi_{2,3}(x)$  as:

$$S_2 : \begin{cases} \Psi_2(x) = F_2(x) + (B_2(x) - B_2(0)) \begin{bmatrix} u_2 \\ u_3 \end{bmatrix} \\ B_2(0) = \begin{bmatrix} \frac{1}{L_{md0}} & 0 \end{bmatrix} \end{cases}, \tag{36}$$

$$S_3 : \begin{cases} \Psi_3(x) = F_3(x) + (B_3(x) - B_3(0)) \begin{bmatrix} u_2 \\ u_3 \end{bmatrix} \\ B_3(0) = \begin{bmatrix} 0 & \frac{1}{L_{mq0}} \end{bmatrix} \end{cases}$$

where  $L_{md0}$  and  $L_{mq0}$ ,  $B_2(0)$  and  $B_3(0)$  are nominal values of  $L_{md}$ ,  $L_{mq}$ ,  $B_2(x)$  and  $B_3(x)$ , respectively.

Defining the state vectors as  $z_{21} = y_2$ ,  $z_{22} = \Psi_2$  and  $z_{31} = y_3$ ,  $z_{32} = \Psi_3$ , and control variables as  $u_2 = V_{md}$  and  $u_3 = V_{mq}$ . The dynamic equations of the two subsystems  $S_2$  and  $S_3$  become as

$$S_2 : \begin{cases} z_{21} = y_2 \\ \dot{z}_{21} = \Psi_2(x) + B_2(0) \begin{bmatrix} u_2 \\ u_3 \end{bmatrix} \\ \dot{z}_{22} = \dot{\Psi}_2(x) \end{cases}, \tag{37}$$

$$S_3 : \begin{cases} z_{31} = y_3 \\ \dot{z}_{31} = \Psi_3(x) + B_3(0) \begin{bmatrix} u_2 \\ u_3 \end{bmatrix} \\ \dot{z}_{32} = \dot{\Psi}_3(x) \end{cases},$$

### 3.2.3. Design of Perturbation Observer

When the system outputs  $y_{2,3}$  are available, two second-order POs are designed for the estimations of states and perturbation for the subsystems

$$S_2 : \begin{cases} \dot{\hat{z}}_{21} &= \hat{z}_{21} + l_{21}(z_{21} - \hat{z}_{21}) + B_2(0)u_2 \\ \dot{\hat{z}}_{22} &= l_{22}(z_{21} - \hat{z}_{21}), \end{cases} \quad (38)$$

$$S_3 : \begin{cases} \dot{\hat{z}}_{31} &= \hat{z}_{31} + l_{31}(z_{31} - \hat{z}_{31}) + B_3(0)u_3 \\ \dot{\hat{z}}_{32} &= l_{32}(z_{31} - \hat{z}_{31}), \end{cases} \quad (39)$$

where  $\hat{z}_{21}$ ,  $\hat{z}_{22}$ ,  $\hat{z}_{31}$ , and  $\hat{z}_{32}$  are the estimations of  $z_{21}$ ,  $z_{22}$ ,  $z_{31}$  and  $z_{32}$ , respectively, and  $l_{21}$ ,  $l_{22}$ ,  $l_{31}$  and  $l_{32}$  are gains of the observers. They are designed similarly to Equation (20).

**Remark 1.** It should be mentioned that during the design procedure,  $\epsilon_i$  used in POs Equations (38) and (39) are required to be some relatively small positive constants only, and the performance of POs is not very sensitive to the observer gains, which are determined based on the upper bound of the derivative of perturbation.

### 3.2.4. Design of Nonlinear Adaptive Controller

The estimated perturbations are used for compensating the real perturbation, and control laws of subsystems  $S_2$  and  $S_3$  can be obtained as follows:

$$\begin{bmatrix} u_2 \\ u_3 \end{bmatrix} = B_2(0)^{-1} \left[ \begin{bmatrix} -\hat{z}_{22} \\ -\hat{z}_{32} \end{bmatrix} + \begin{bmatrix} v_2 \\ v_3 \end{bmatrix} \right] \quad (40)$$

where  $v_{2,3}$  is defined as

$$\begin{cases} v_2 &= k_{21}(z_{21r} - \hat{z}_{21}) + \dot{z}_{21r} \\ v_3 &= k_{31}(z_{31r} - \hat{z}_{31}) + \dot{z}_{31r} \end{cases} \quad (41)$$

The final control law represented by currents and inductances, are expressed as follows:

$$\begin{cases} u_2 = L_{md0}[k_{21}(i_{mdr} - i_{md}) + \dot{i}_{mdr} - \hat{\Psi}_2] \\ u_3 = L_{mq0}[k_{31}(i_{mqr} - i_{mq}) + \dot{i}_{mqr} - \hat{\Psi}_3] \end{cases} \quad (42)$$

Please note that only the nominal values of  $L_{md0}$ ,  $L_{mq0}$ , and measurements of  $i_{md}$  and  $i_{mq}$  are required in the NAC design.

To clearly illustrate its principle, Figure 4 shows the block diagram of the NAC.

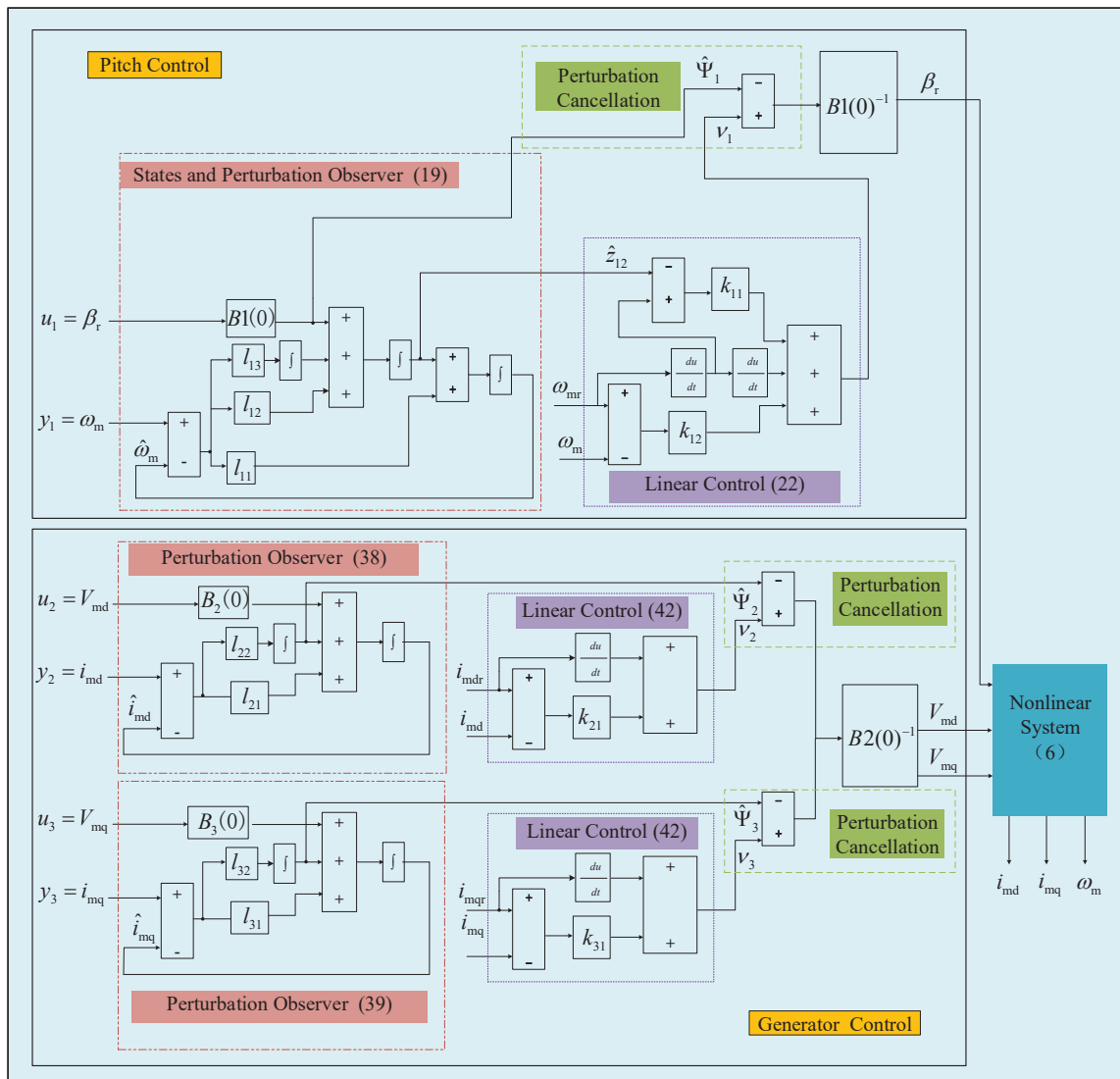


Figure 4. Block diagram of nonlinear adaptive controller.

The following assumptions are made in [19,21,36–39].

**Assumption 1.** Input gain  $B(x)$  and its derivative are bounded by  $0 < M_1 \leq B(x) \leq M_2$ ,  $|\dot{B}(x)| \leq M_3$ , where  $M_i$ ,  $i = 1, 2, 3$  are finite constants [for convenience we assume that  $B(x) > 0$ ].  $B(0)$  is chosen to satisfy:  $|B(x)/B(0) - 1| \leq \theta < 1$ , where  $\theta$  is a positive constant. The control  $u$  is assumed to be bounded but big enough for the purpose of perturbation cancellation.

**Assumption 2.** The perturbation  $\Psi_i(x, t)$  and its derivative  $\dot{\Psi}_i(x, t)$  are locally Lipschitz in their arguments and bounded over the domain of interest.

### 3.2.5. Stability Analysis of Closed-Loop System

This subsection analyzes the stability of the closed-loop system equipped with the NAC designed in the previous section.

At first, both the estimation error system and the tracking error system are obtained. On one hand, by defining estimation errors  $\varepsilon_{21} = z_{21} - \hat{z}_{21}$ ,  $\varepsilon_{22} = z_{22} - \hat{z}_{22}$ ,  $\varepsilon_{31} = z_{31} - \hat{z}_{31}$ ,  $\varepsilon_{32} = z_{32} - \hat{z}_{32}$ ,

subtracting Equation (38) from Equation (37) and subtracting Equation (39) from Equation (37), the following estimation error system yields:

$$\dot{\varepsilon}_i = A_i \varepsilon_i + \eta_i \tag{43}$$

where

$$\varepsilon_i = \begin{bmatrix} \varepsilon_{21} \\ \varepsilon_{22} \\ \varepsilon_{31} \\ \varepsilon_{32} \end{bmatrix}, \quad \eta_i = \begin{bmatrix} 0 \\ \Psi_2 \\ 0 \\ \Psi_3 \end{bmatrix},$$

$$A_i = \begin{bmatrix} -l_{21} & 1 & 0 & 0 \\ -l_{22} & 0 & 0 & 0 \\ 0 & 0 & -l_{31} & 1 \\ 0 & 0 & -l_{32} & 0 \end{bmatrix} \tag{44}$$

On the other hand, define the tracking errors as  $e_{21} = y_{2r} - z_{21}$  and  $e_{31} = y_{3r} - z_{31}$ . It follows from Equations (24), (26), (36), (40) and (41) that

$$\begin{bmatrix} \dot{e}_{21} \\ \dot{e}_{31} \end{bmatrix} = - \begin{bmatrix} k_{21}(e_{21} + \varepsilon_{21}) + \varepsilon_{22} \\ k_{31}(e_{31} + \varepsilon_{31}) + \varepsilon_{32} \end{bmatrix} \tag{45}$$

Thus, the tracking error system can be summarized as

$$\dot{e}_i = M_i e_i + \vartheta_i \tag{46}$$

where

$$e_i = \begin{bmatrix} e_{21} \\ e_{22} \end{bmatrix}, \quad \vartheta_i = \begin{bmatrix} -\zeta_1 \\ -\zeta_2 \end{bmatrix},$$

$$M_i = \begin{bmatrix} -k_{21} & 0 \\ 0 & -k_{31} \end{bmatrix} \tag{47}$$

with  $\zeta_1 = \varepsilon_{22} + k_{21}\varepsilon_{21}$  and  $\zeta_2 = \varepsilon_{32} + k_{31}\varepsilon_{31}$  being the lumped estimation error.

The stability analysis of the closed-loop control system is transformed into globally uniformly ultimately bounded summarized.

**Theorem 1.** Consider the PMSM system Equation (24) equipped the proposed NAC Equation (42) with two POs Equations (38) and (39). If the real perturbation  $\Psi_i(x, t)$  defined in Equation (36) satisfies

$$\|\Psi_i(x, t)\| \leq \gamma_1 \tag{48}$$

then both the estimation error system Equation (43) and the tracking error system Equation (46) are, i.e.,

$$\|\varepsilon_i(t)\| \leq 2\gamma_1 \|P_1\|, \|e_i(t)\| \leq 4\gamma_1 \|K_i\| \|P_1\| \|P_2\|, \forall t \geq T \tag{49}$$

where  $P_i, i = 1, 2$  are respectively the feasible solutions of Riccati equations  $A_i^T P_1 + P_1 A_i = -I$  and  $M_i^T P_2 + P_2 M_i = -I$ ; and  $\|K_i\|$  is a constant related to  $k_{11}, k_{21}$  and  $k_{22}$ .

**Proof.** For the estimation error system Equation (43), consider the following Lyapunov function:

$$V_{i1}(\varepsilon_i) = \varepsilon_i^T P_1 \varepsilon_i \tag{50}$$

The high gains of POs Equations (38) and (39) are determined by requiring Equation (21) holds, which means  $A_i$  is Hurwitz. One can find a feasible positive definite solution,  $P_1$ , of Riccati equation  $A_i^T P_1 + P_1 A_i = -I$ . Calculating the derivative of  $V_{i1}(\varepsilon_i)$  along the solution of system Equation (43) and using Equation (48) to yield

$$\begin{aligned} \dot{V}_{i1}(\varepsilon_i) &= \varepsilon_i^T (A_i^T P_1 + P_1 A_i) \varepsilon_i + \eta_i^T P_1 \varepsilon_i + \varepsilon_i^T P_1 \eta_i \\ &\leq -\|\varepsilon_i\|^2 + 2\|\varepsilon_i\| \cdot \|\eta_i\| \cdot \|P_1\| \\ &\leq -\|\varepsilon_i\|(\|\varepsilon_i\| - 2\gamma_1 \|P_1\|) \end{aligned} \tag{51}$$

Then  $\dot{V}_{i1}(\varepsilon_i) \leq 0$  when  $\|\varepsilon_i\| \geq 2\gamma_1 \|P_1\|$ . Thus, there exists  $T_1 > 0$ , which can lead to

$$\|\varepsilon_i(t)\| \leq \gamma_2 = 2\gamma_1 \|P_1\|, \forall t \geq T_1 \tag{52}$$

For tracking error system Equation (46), one can find that  $\|\theta_i\| \leq \|K_i\| \gamma_2$  with  $\|K_i\|$  based on  $\|\varepsilon_i(t)\| \leq \gamma_2$ . Consider the Lyapunov function  $V_{i2}(e_i) = e_i^T P_2 e_i$ . Similarly, one can prove that there exists an instant,  $T_1$ , the following holds

$$\|e_i(t)\| \leq 2\|K_i\| \gamma_2 \|P_2\| \leq 4\gamma_1 \|K_i\| \|P_1\| \|P_2\|, \forall t \geq \bar{T}_1 \tag{53}$$

Using Equations (52) and (53) and setting  $T = \max\{T_1, \bar{T}_1\}$  lead to Equation (49).

Moreover, if  $\Psi_i(x, t)$  and  $\dot{\Psi}_i(x, t)$  are locally Lipschitz in their arguments, it will guarantee the exponential convergence of the observation error [19] and closed-loop tracking error into

$$\lim_{t \rightarrow \infty} \varepsilon_i(t) = 0 \quad \text{and} \quad \lim_{t \rightarrow \infty} e_i(t) = 0 \tag{54}$$

After the states  $i_d$  and  $i_q$  and their derivatives are stable that controlled by NAC. The parameter variation is considered in the error system in Equations (43) and (46), and the error system is proved as converged to zero in Equation (54). This guarantees that the estimated perturbations track the extended states defined in Equation (36), which includes the uncertainties affected by the parameter variations and disturbances, and compensates for the control input in Equation (40). Then the linearized subsystems in Equation (37) are independent of the parameters and disturbances.  $\square$

**Remark 2.** The perturbation and its derivative are assumed to locally bounded as described in **Assumption 2**. The existence of these bounds can be shown in the following analysis. The perturbation and its derivative can be represented as

$$\begin{aligned} \Psi_2 &= F_2(x) + \frac{B_2(x) - B_2(0)}{B_2(x)} [k_{21}(z_{21r} - z_{21}) + z_{22} - \hat{z}_{22}] \\ &= F_2(x) + \frac{B_2(x) - B_2(0)}{B_2(x)} (k_{21}e_{21} + \varepsilon_{22}) \\ \dot{\Psi}_2 &= \dot{F}_2(x) + \frac{B_2(x) - B_2(0)}{B_2(0)} (-\dot{\Psi}_2 + k_{21}\dot{e}_{21} - \dot{\varepsilon}_{22}) \\ &= \dot{F}_2(x) + \frac{B_2(x) - B_2(0)}{B_2(0)} (k_{21}\dot{e}_{21} + l_{22}\varepsilon_{21}) \\ \Psi_3 &= F_3(x) + \frac{B_3(x) - B_3(0)}{B_3(x)} [k_{31}(z_{31r} - z_{31}) + z_{32} - \hat{z}_{32}] \\ &= F_3(x) + \frac{B_3(x) - B_3(0)}{B_3(x)} (k_{31}e_{31} + \varepsilon_{32}) \\ \dot{\Psi}_3 &= \dot{F}_3(x) + \frac{B_3(x) - B_3(0)}{B_3(0)} (-\dot{\Psi}_3 + k_{31}\dot{e}_{31} - \dot{\varepsilon}_{32}) \\ &= \dot{F}_3(x) + \frac{B_3(x) - B_3(0)}{B_3(0)} (k_{31}\dot{e}_{31} + l_{32}\varepsilon_{31}) \end{aligned}$$

Considering **Assumption 1**, we have

$$\begin{aligned}
 |\Psi_2| &\leq \frac{1}{1-\theta_2} |F_2(x)| + \frac{\theta_2}{1+\theta_2} (\|k_{21}\| \|e_{21}\| + |\varepsilon_{22}|) \\
 |\dot{\Psi}_2| &\leq |\dot{F}_2(x)| + |B_2(x)| \|u_2\| + \theta_2 (\|k_{21}\| \|\dot{e}_{21}\| + l_{22} |\varepsilon_{21}|) \\
 |\Psi_3| &\leq \frac{1}{1-\theta_3} |F_3(x)| + \frac{\theta_3}{1+\theta_3} (\|k_{31}\| \|e_{31}\| + |\varepsilon_{32}|) \\
 |\dot{\Psi}_3| &\leq |\dot{F}_3(x)| + |B_3(x)| \|u_3\| + \theta_3 (\|k_{31}\| \|\dot{e}_{31}\| + l_{32} |\varepsilon_{31}|)
 \end{aligned}$$

From the above equations, with consideration of the perturbation assumed as a smooth function of time, it can be concluded that the bound of perturbation and its derivative exist.

As a result, with both the **Assumptions 1 and 2**, the effectiveness of such perturbation observer-based control can be guaranteed.

#### 4. Simulation Results

To verify the effectiveness of the proposed NAC, simulations studies (Matlab/Simulink) have been carried out by comparing with the VC, GSPI and FLC. In this paper, a 2 MW PMSG-WT given in [35] is investigated. The parameters of the PMSG-WT system are listed in Table 1. In this paper, the mechanical rotation speed reference is  $\omega_{mr} = 2.2489$  rad/s. The reference of d-axis stator current is  $i_{m\text{dr}} = 0$  A. The rated electromagnetic torque reference is  $T_{er} = 889326.7$  Nm. According to Equation (7), the q-axis stator current reference is  $i_{m\text{qr}} = 593.3789$  A.

**Table 1.** Parameters of PMSG-WT for simulation studies.

Parameters	Values	Units
Air density $\rho$	1.205	kg/m <sup>3</sup>
Rated wind speed $V_r$	12	m/s
Blade radius $R$	39	m
Actuator time constant $\tau_\beta$	1	s
pitch angle rate $\beta_{\text{rate}}$	$\pm 10$	degree/s
Rated output power $P_r$	2	MW
Stator resistance $R_s$	50	$\mu\Omega$
d-axis inductance $L_d$	5.5	mH
q-axis inductance $L_q$	3.75	mH
Number of pole pairs $p$	11	
Field flux $K_e$	136.25	V · s/rad
Total inertia $J_{\text{tot}}$	10,000	kg · m <sup>2</sup>

Parameters of NACs for subsystems  $S_1$ ,  $S_2$ , and  $S_3$  are designed based on pole-placement and listed in Table 2. Please note that the controller parameters of the FLC are the same as that of the NAC for all three subsystems, and the FLC requires exact system parameters and full state measurements except  $\frac{dV}{dt}$ .

**Table 2.** Parameters of Pitch control approach for simulation studies.

Parameters of the NAC Equation (42)	
Gains of observer Equation (19)	$\alpha_{11} = 50, \alpha_{12} = 1.875 \times 10^3, \alpha_{13} = 1.5625 \times 10^4, \epsilon_1 = 0.02$
Gains of observer Equation (38)	$\alpha_{21} = 4 \times 10^2, \alpha_{22} = 4 \times 10^4, \epsilon_2 = 0.01$
Gains of observer Equation (39)	$\alpha_{31} = 4 \times 10^2, \alpha_{32} = 4 \times 10^4, \epsilon_3 = 0.01$
Gains of linear controller Equation (41)	$k_{11} = 40, k_{12} = 4 \times 10^2, k_{21} = 1.6 \times 10^2, k_{31} = 1.6 \times 10^2$

4.1. Ramp Wind

Figures 5 and 6 show the responses of the PMSG-WT to ramp wind. Wind speed is shown in Figure 5a. As shown in Figure 5b,c, the proposed NAC provides the smallest tracking error of the mechanical rotation speed  $\omega_m$ , compared with the VC, GSPI and FLC. The VC has the biggest tracking error and requires the longest recovery time. It can be explained that the VC is adjusted for a specific operation point of the system and cannot ensure provision of a satisfactory dynamic performance for time-varying operation points. Although the FLC can provide a high tracking performance, the tracking error of  $\omega_m$  still exists. It is because that the FLC requires full state measurements, but the  $\frac{dV}{dt}$  in Equation (9) is unknown in the FLC design. The GSPI also achieves better performance than the VC. This is because the GSPI can schedule PI gains frequently under time-varying wind speeds. However, it increases the burden of the controller.

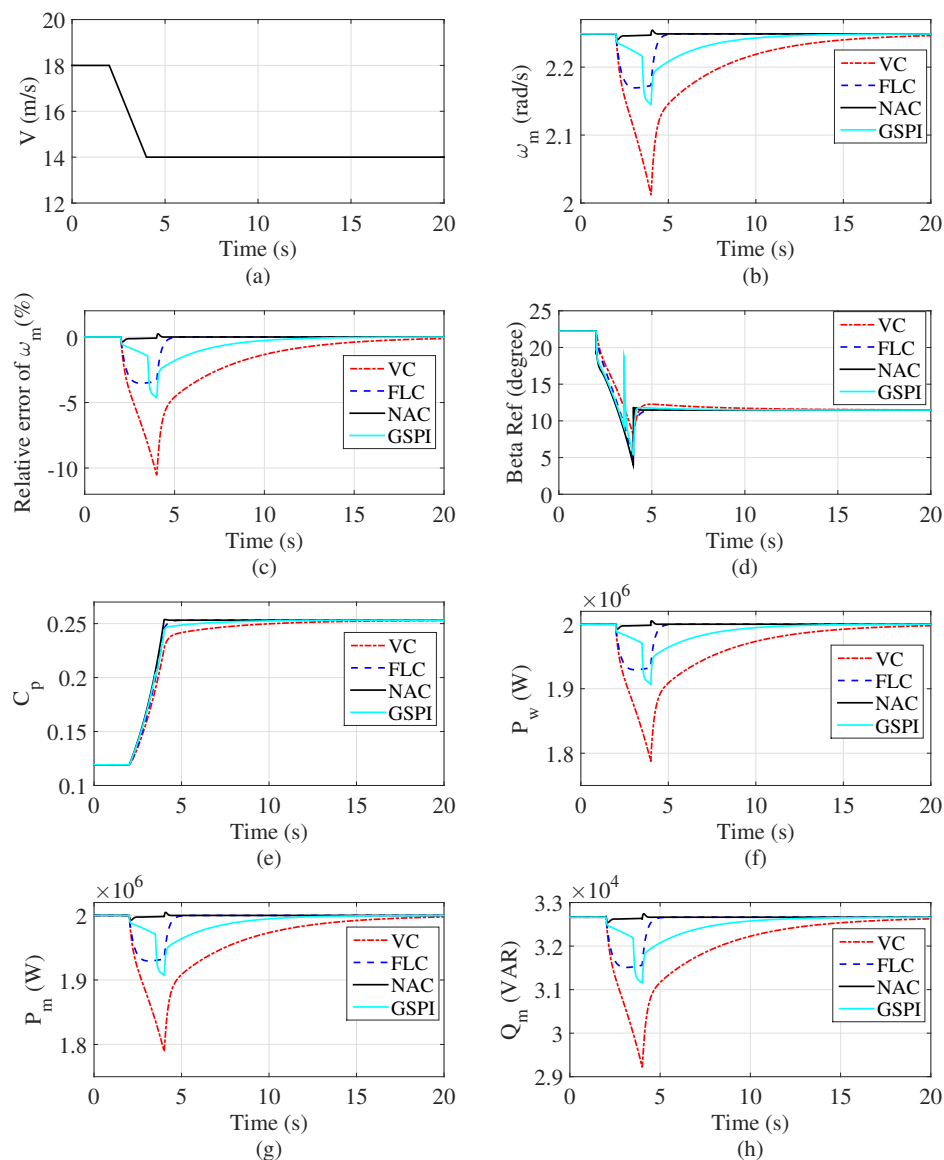


**Figure 5.** Responses of the PMSG-WT to ramp wind speed. (a) Wind speed  $V$ . (b) Mechanical rotation speed  $\omega_m$ . (c) Relative error of  $\omega_m$ . (d) Required pitch angle. (e) Power coefficient  $C_p$ . (f) Mechanical power  $P_w$ . (g) Active generating power  $P_m$ . (h) Reactive generating power  $Q_m$ .

To keep the extracted wind power at the rated power, the required pitch angle  $\beta_r$  should change with the varying wind speed, as shown in Figure 5d. In Figure 5e,f, to maintain the extracted

wind power around its rated value, the power coefficient  $C_p$  increases when wind speed decreases. The extracted wind power can be maintained around its rated value under the NAC even when wind speed varies, which the VC, GSPI and FLC cannot provide. The active generating power  $P_m$  and reactive generating power  $Q_m$  of the PMSG-WT are shown in Figure 5g,h, respectively.

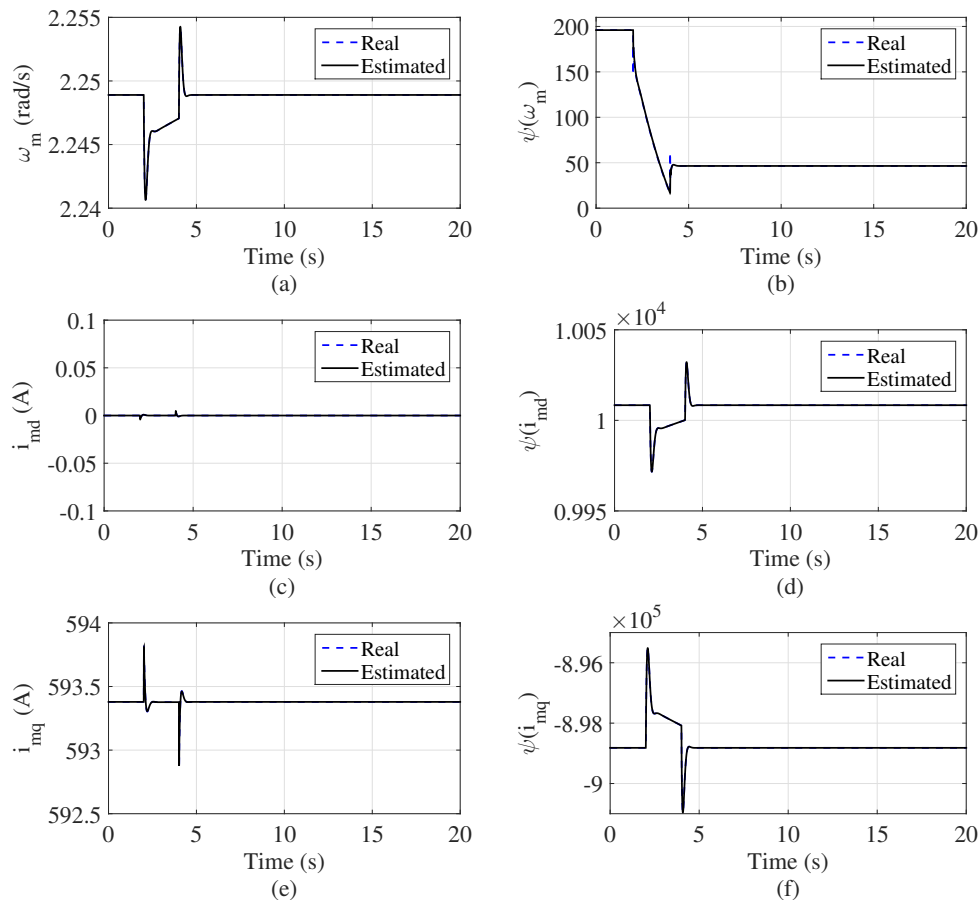


**Figure 6.** Estimations of states and perturbations. (a) Estimation of mechanical rotation speed  $\omega_m$ . (b) Estimation of perturbation term  $\Psi_1$ . (c) Estimation of  $i_{md}$ . (d) Estimation of perturbation term  $\Psi_2$ . (e) Estimation of  $i_{mq}$ . (f) Estimation of perturbation term  $\Psi_3$ .

In the previous section, it mentions that the proposed NAC can estimate the defined perturbation terms Equations (17) and (36) via the designed observers Equations (19), (38) and (39) to compensate the real perturbation. It can be seen from Figure 6 that both the states and perturbations can be well estimated by the designed SPO.

#### 4.2. Random Wind

Figures 7 and 8 show the responses of the PMSG-WT to random wind. Figure 7a shows time-varying wind speed. It can be seen from Figure 7b,c that the VC, GSPI and FLC cannot provide high tracking performance of the mechanical rotation speed  $\omega_m$  under time-varying wind speed. However, the GSPI achieve better tracking performance than the FLC under random wind speeds. The NAC always keeps mechanical rotation speed  $\omega_m$  around its rated value. To limit the extracted wind power, the power coefficient  $C_p$  varies with time-varying wind speed, shown in Figure 7d. During the whole operating period, the NAC can always keep consistent responses of  $P_m$  and  $Q_m$  shown in Figure 7e,f. The performances of the VC, GSPI and FLC are all affected by the time-varying wind speed. Figure 8 shows the designed observers can provide satisfactory estimations for the states and perturbations.

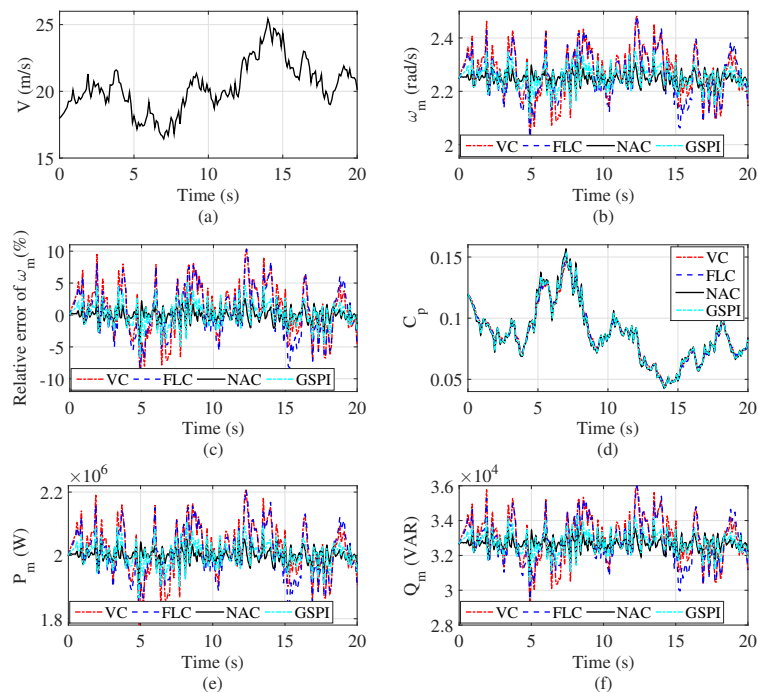


**Figure 7.** Responses of the PMSG-WT to random wind speed. (a) Wind speed  $V$ . (b) Mechanical rotation speed  $\omega_m$ . (c) Relative error of  $\omega_m$ . (d) Power coefficient  $C_p$ . (e) Active generating power  $P_m$ . (f) Reactive generating power  $Q_m$ .

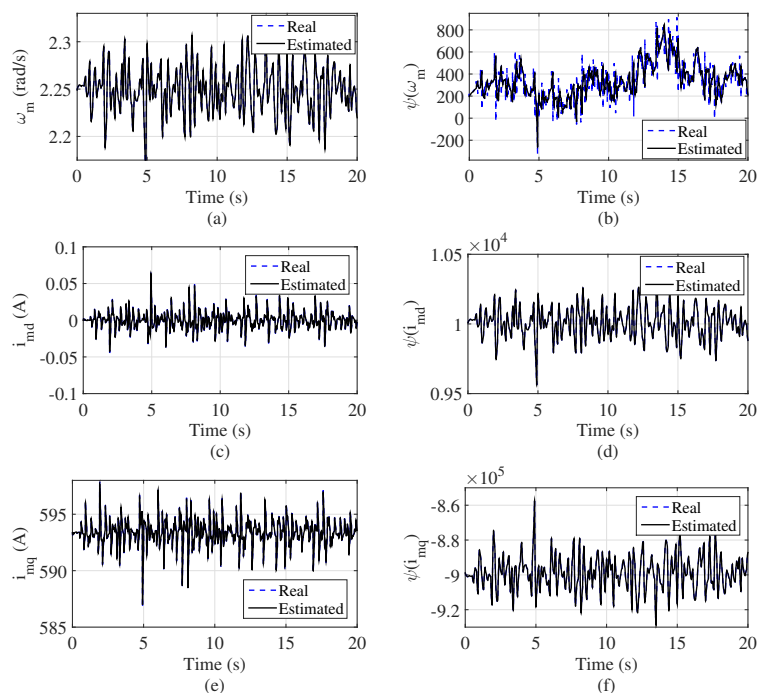


**Figure 8.** Estimations of states and perturbations. (a) Estimation of mechanical rotation speed  $\omega_m$ . (b) Estimation of perturbation term  $\Psi_1$ . (c) Estimation of  $i_{md}$ . (d) Estimation of perturbation term  $\Psi_2$ . (e) Estimation of  $i_{mq}$ . (f) Estimation of perturbation term  $\Psi_3$ .

### 4.3. Robustness Against Parameter Uncertainty

For a practical PMSG-WT system, the operating temperature, manufacturing tolerance and magnetic saturation effect may result in the variation of system parameter values. The control

performance of the VC, FLC and proposed NAC is tested under field flux variation. Please note that the wind speed is kept at 18 m/s. The variation of field flux  $K_e$  is shown in Figure 9a.

In Figure 9b, the proposed NAC can provide better tracking performance of the mechanical rotation speed  $\omega_m$ , compared with the VC and FLC. The maximum relative error ( $\frac{\omega_m - \omega_{mr}}{\omega_{mr}} \times 100\%$ ) reaches approximately 5% and 1% under the FLC and VC, respectively. The control performance of the VC and FLC are both affected by field flux variation. In Figure 9c,d, the responses of the required pitch angle  $\beta_r$  and power coefficient  $C_p$  are shown. The active generating power  $P_m$  and reactive generating power  $Q_m$  of the PMSG-WT are shown in Figure 9e,f, respectively. The active generation power  $P_m$  cannot be kept at its rated value under these three controllers, especially under the FLC. The reactive generating power  $Q_m$  is almost unaffected under the NAC.

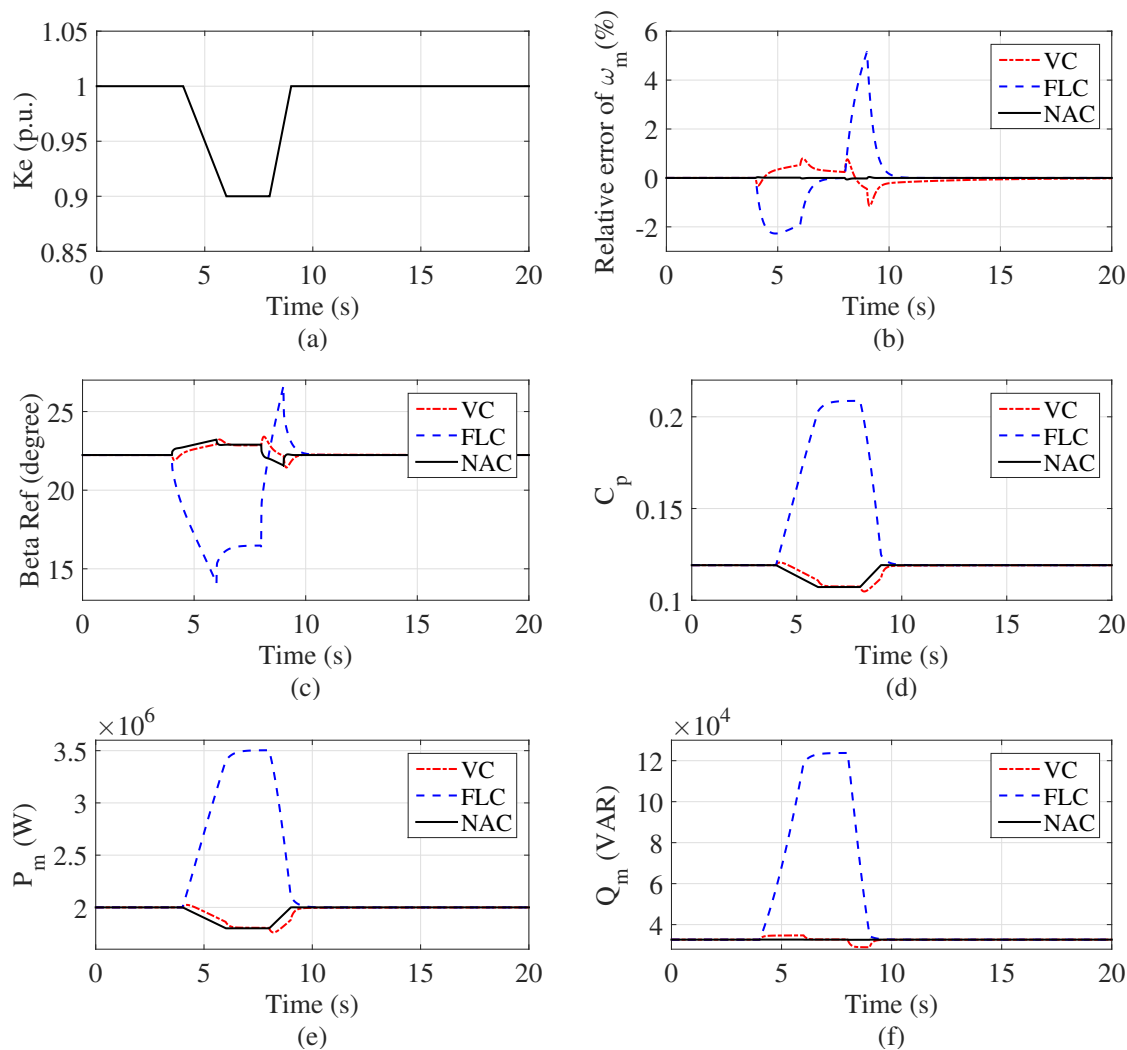


**Figure 9.** Response to field flux  $K_e$  variation under constant wind speed. (a) Variation of field flux  $K_e$ . (b) Relative error of mechanical rotation speed  $\omega_m$ . (c) Required pitch angle. (d) Power coefficient  $C_p$ . (e) Active generating power  $P_m$ . (f) Reactive generating power  $Q_m$ .

In addition, Table 3 shows the control performance of these three controllers via integral of absolute error (IAE) in different simulation scenarios. Here,  $IAE_x = \int_0^T |x - x^*|$ . The reference value of the variable  $x$  is  $x^*$ . The simulation time  $T$  is set as 20 s. It can be seen from Table 3 that in first and second simulation scenarios, the  $IAE_{i_d}$  and  $IAE_{i_q}$  are both almost around 0 A.s under these three controllers. Compared with the VC and FLC, the  $IAE_{\omega_m}$  is smaller under the proposed NAC. In the field flux variation simulation scenario, the NAC can provide much smaller  $IAE_{i_q}$  and  $IAE_{\omega_m}$  than

those achieved by the VC and FLC. Compare with the VC, the FLC is more significantly affected by field flux variation.

The proposed NAC can always provide a satisfactory performance. This is because the proposed NAC can estimate all uncertainties without knowing detailed system model. Therefore, it has better robustness than the FLC, which requires accurate system parameters. Meanwhile, the control performance of the VC is affected under parameter variations [29].

**Table 3.** IAE indices of different controllers in different scenarios.

Simulation Scenarios	Variables	Controllers		
		VC	FLC	NAC
Ramp wind speed	$IAE_{\omega_m}$ (rad)	0.817	0.1555	$1.397 \times 10^{-5}$
	$IAE_{i_d}$ (A · s)	$9.603 \times 10^{-15}$	$1.025 \times 10^{-13}$	$3.076 \times 10^{-5}$
	$IAE_{i_q}$ (A · s)	$8.634 \times 10^{-13}$	$6.972 \times 10^{-12}$	$2.752 \times 10^{-3}$
Random wind speed	$IAE_{\omega_m}$ (rad)	1.369	1.273	$1.514 \times 10^{-3}$
	$IAE_{i_d}$ (A · s)	$9.98 \times 10^{-15}$	$1.075 \times 10^{-13}$	$6.75 \times 10^{-3}$
	$IAE_{i_q}$ (A · s)	$9.598 \times 10^{-13}$	$7.154 \times 10^{-12}$	0.6171
Field flux variation	$IAE_{\omega_m}$ (rad)	0.0695	0.207	$2.995 \times 10^{-6}$
	$IAE_{i_d}$ (A · s)	$9.526 \times 10^{-15}$	$1.24 \times 10^{-13}$	$1.852 \times 10^{-5}$
	$IAE_{i_q}$ (A · s)	67.78	1957	0.04528

## 5. Conclusions

This paper has developed a nonlinear adaptive pitch controller for the PMSG-WT to limit the extracted power from time-varying wind in Region 3. In the proposed NAC, all time-varying and unknown dynamics of the PMSG-WT, e.g., nonlinearities, parameter uncertainties and disturbances, are included by defined perturbation terms, which are estimated by designed POs and SPO. The estimated perturbations are used to compensate the real perturbations for fully linearizing the PMSG-WT system. The proposed NAC has overcome the drawbacks of the FLC relying on the full system states and detailed nonlinear system model, the shortcoming of the VC designed based on a specific operating point, and the disadvantages of the GSPI scheduling PI gains frequently under time-varying wind speeds. Simulation studies are carried out for the comparison of the control performance achieved by the VC, FLC, GSPI and NAC under different scenarios. Compared with the FLC, GSPI and VC, the proposed NAC provides the best performance under different scenarios and achieves highest robustness against field flux variation. Wind speed sensorless control approach will be focused on in further work. The effective wind speed cannot be directly measured by anemometers, but it can be estimated through employing the WT itself as a wind speed measurement device [8].

**Author Contributions:** Conceptualization, J.C. and B.Y.; validation, J.C. and B.Y.; investigation, J.C. and W.D.; methodology, T.Y. and N.A.; writing—original draft preparation, J.C.; writing—review and editing, W.D. and B.Y.; visualization, H.S. and L.C.; supervision, H.S. and L.C.; project administration, J.C., B.Y. and T.Y.; funding acquisition, J.C., B.Y. and T.Y.

**Funding:** This research was funded by the Natural Science Foundation of the Jiangsu Higher Education Institutions of China (Grant No. 19KJB470036), National Natural Science Foundation of China grant number (Grant Nos. 51667010, 51777078), the Fundamental Research Funds for the Central Universities (Grant No. D2172920), the Key Projects of Basic Research and Applied Basic Research in Universities of Guangdong Province (Grant No. 2018KZDXM001), and the Science and Technology Projects of China Southern Power Grid (Grant No. GDKJXM20172831).

**Conflicts of Interest:** The authors declare no conflict of interest.

## References

1. Aissaoui, A.G.; Tahour, A.; Essounbouli, A.; Nollet, F.; Abid M.; Chergui, M.I. A fuzzy-PI control to extract an optimal power from wind turbine. *Energy Convers. Manag.* **2013**, *65*, 688–696. [[CrossRef](#)]
2. Chen, J.; Yao, W.; Zhang, C.K.; Ren, Y.X.; Jiang, L. Design of robust MPPT controller for grid-connected PMSG-Based wind turbine via perturbation observation based nonlinear adaptive control. *Renew. Energy* **2019**, *134*, 478–495. [[CrossRef](#)]
3. Liao, S.W.; Yao, W.; Han, X.N.; Wen, J.Y.; Cheng, S.J. Chronological operation simulation framework for regional power system under high penetration of renewable energy using meteorological data. *Appl. Energy* **2017**, *203*, 816–828. [[CrossRef](#)]
4. Yang, B.; Jiang, L.; Yao, W.; Wu, Q.H. Nonlinear maximum power point tracking control and modal analysis of DFIG based wind turbine. *Int. J. Electr. Power Energy Syst.* **2016**, *74*, 429–436. [[CrossRef](#)]
5. Liu, J.; Yao, W.; Wen, J.Y.; Fang, J.K.; Jiang, L.; He, H.B.; Cheng, S.J. Impact of power grid strength and PLL parameters on stability of grid-connected DFIG wind farm. *IEEE Trans. Sustain. Energy* **2019**. [[CrossRef](#)]
6. Yang, B.; Zhang, X.S.; Yu, T.; Shu, H.C.; Fang, Z.H. Grouped grey wolf optimizer for maximum power point tracking of doubly-fed induction generator based wind turbine. *Energy Convers. Manag.* **2017**, *133*, 427–443. [[CrossRef](#)]
7. Abdullah, M.A.; Yatim, A.H.M.; Tan, C.W.; Saidur, R. A review of maximum power point tracking algorithms for wind energy systems. *Renew. Sustain. Energy Rev.* **2012**, *16*, 3220–3227. [[CrossRef](#)]
8. Kumar, A.; Stol, K. Simulating feedback linearization control of wind turbines using high-order models. *Wind Energy* **2009**, *13*, 419–432. [[CrossRef](#)]
9. Boukhezzar, B.; Siguerdidjane, H. Nonlinear Control of a variable-speed wind turbine using a two-mass model. *IEEE Trans. Energy Convers.* **2011**, *26*, 149–162. [[CrossRef](#)]
10. Van, T.L.; Nguyem, T.H.; Lee, D.C. Advanced pitch angle control based on fuzzy logic for variable-speed wind turbine systems. *IEEE Trans. Energy Convers.* **2015**, *30*, 578–587. [[CrossRef](#)]
11. Boukhezzar, B.; Lupu, L.; Siguerdidjane, H.; Hand, M. Multivariable control strategy for variable speed, variable pitch wind turbines. *Renew. Energy* **2007**, *32*, 1273–1287. [[CrossRef](#)]
12. Connor, B.; Leithead, W.E.; Grimble, M. LQG control of a constant speed horizontal axis wind turbine. *Proc. IEEE CCA* **1994**, *1*, 251–252.
13. Bossanyi, E.A. The design of closed loop controllers for wind turbines. *Wind Energy* **2000**, *3*, 149–163. [[CrossRef](#)]
14. Akhmatov, V.; Knudsen, H.; Nielsen, A.H.; Pedersen, J.K.; Poulsen, N.J. Modelling and transient stability of large wind farms. *Int. J. Electr. Power Energy Syst.* **2003**, *25*, 123–144. [[CrossRef](#)]
15. Pao, L.; Johnson, K. A tutorial on the dynamics and control of wind turbines and wind farms. *Proc. ACC* **2009**. [[CrossRef](#)]
16. Mullane, A.; Lightbody, G.; Yacamini, R. Wind-turbine fault ride-through enhancement. *IEEE Trans. Power Syst.* **2005**, *20*, 1929–1937. [[CrossRef](#)]
17. Seol, J.Y.; Ha, I.J. Feedback-linearizing control of IPM motors considering magnetic saturation effect. *IEEE Trans. Power Electron.* **2005**, *20*, 416–424. [[CrossRef](#)]
18. Kim, K.H.; Jeung, Y.C.; Lee, D.C.; Kim, H.J. LVRT strategy of PMSG wind power systems based on feedback linearization. *IEEE Trans. Power Electron.* **2012**, *27*, 2376–2384. [[CrossRef](#)]
19. Jiang, L.; Wu, Q.H. Nonlinear adaptive control via sliding-mode state and perturbation observer. *IEEE Proc. Control Theory Appl.* **2002**, *149*, 269–277. [[CrossRef](#)]
20. Mauricio, J.M.; Leon, A.E.; Gomez-Exposito, A.; Solsona, J.A. An adaptive nonlinear controller for DFIM-based wind energy conversion systems. *IEEE Trans. Energy Convers.* **2008**, *23*, 1024–1035. [[CrossRef](#)]
21. Yang, B.; Yu, T.; Shu, H.C.; Dong, J.; Jiang, L. Robust sliding-mode control of wind energy conversion systems for optimal power extraction via nonlinear perturbation observers. *Appl. Energy* **2018**, *210*, 711–723. [[CrossRef](#)]
22. Noureldeen, O.; Hamdan, I. Design of robust intelligent protection technique for large-scale grid-connected wind farm. *Prot. Control Mod. Power Syst.* **2018**, *3*, 169–182. [[CrossRef](#)]
23. Shen, Y.; Yao, W.; Wen, J.Y.; He, H.B.; Jiang, L. Resilient wide-area damping control using GrHDP to tolerate communication failures. *IEEE Trans. Smart Grid* **2019**, *10*, 2547–2557. [[CrossRef](#)]

24. Han, B.; Zhou, L.W.; Yang, F.; Xiang, Z. Individual pitch controller based on fuzzy logic control for wind turbine load mitigation. *IET Renew. Power Gener.* **2016**, *10*, 687–693. [[CrossRef](#)]
25. Liu, J.; Wen, J.Y.; Yao, W.; Long, Y. Solution to short-term frequency response of wind farms by using energy storage systems. *IET Renew. Power Gener.* **2016**, *10*, 669–678. [[CrossRef](#)]
26. Saravanakumar, R.; Jena, D. Validation of an integral sliding mode control for optimal control of a three blade variable speed variable pitch wind turbine. *Int. J. Electr. Power Energy Syst.* **2015**, *69*, 421–429. [[CrossRef](#)]
27. Saravanakumar, R.; Jena, D. Modified vector controlled DFIG wind energy system based on barrier function adaptive sliding mode control. *Prot. Control Mod. Power Syst.* **2019**, *4*, 34–41.
28. Lin, W.M.; Hong, C.M. A new Elman neural network-based control algorithm for adjustable-pitch variable-speed wind-energy conversion systems. *IEEE Trans. Power Electron.* **2011**, *26*, 473–481. [[CrossRef](#)]
29. Chen, J.; Jiang, L.; Yao, W.; Wu, Q.H. Perturbation estimation based nonlinear adaptive control of a full-rated converter wind-turbine for fault ride-through capability enhancement. *IEEE Trans. Power Syst.* **2014**, *29*, 2733–2743. [[CrossRef](#)]
30. Chen, J.; Yao, W.; Ren, Y.X.; Wang, R.T.; Zhang, L.H.; Jiang, L. Nonlinear adaptive speed control of a permanent magnet synchronous motor: A perturbation estimation approach. *Control Eng. Pract.* **2019**, *85*, 163–175. [[CrossRef](#)]
31. Yang, B.; Yu, T.; Shu, H.C.; Zhang, Y.M.; Chen, J.; Sang, Y.Y.; Jiang, L. Passivity-based sliding-mode control design for optimal power extraction of a PMSG based variable speed wind turbine. *Renew. Energy* **2018**, *119*, 577–589. [[CrossRef](#)]
32. Yang, B.; Yu, T.; Shu, H.C.; Zhu, D.N.; Zeng, F.; Sang, Y.Y.; Jiang, L. Perturbation observer based fractional-order PID control of photovoltaics inverters for solar energy harvesting via Yin-Yang-Par optimization. *Energy Convers. Manag.* **2018**, *171*, 170–187. [[CrossRef](#)]
33. Ren, Y.X.; Li, L.Y.; Brindley, J.; Jiang, L. Nonlinear PI control for variable pitch wind turbine. *Control Eng. Pract.* **2016**, *50*, 84–94. [[CrossRef](#)]
34. Xia, Y.; Ahmed, K.H.; Williams, B.W. A new maximum power point tracking technique for permanent magnet synchronous generator based wind energy conversion system. *IEEE Trans. Power Electron.* **2011**, *26*, 3609–3620. [[CrossRef](#)]
35. Uehara, A.; Pratap, A.; Goya, T.; Senjyu, T.; Yona, A.; Urasaki, N.; Funabashi, T. A coordinated control method to smooth wind power fluctuations of a PMSG-based WECS. *IEEE Trans. Energy Convers.* **2011**, *26*, 550–558. [[CrossRef](#)]
36. Jiang, L.; Wu, Q.H.; Wen, J.Y. Decentralized nonlinear adaptive control for multimachine power systems via high-gain perturbation observer. *IEEE Trans. Circuits Syst. I Regul. Pap.* **2004**, *51*, 2052–2059. [[CrossRef](#)]
37. Youcef, K.; Wu, S. Input/output linearization using time delay control. *J. Dyn. Syst. Meas. Control* **1992**, *114*, 10–19. [[CrossRef](#)]
38. Yang, B.; Jiang, L.; Yao, W.; Wu, Q.H. Perturbation estimation based coordinated adaptive passive control for multimachine power systems. *Control Eng. Pract.* **2015**, *44*, 172–192. [[CrossRef](#)]
39. Wu, Q.H.; Jiang, L.; Wen, J.Y. Decentralized adaptive control of interconnected non-linear systems using high gain observer. *Int. J. Control* **2004**, *77*, 703–712. [[CrossRef](#)]

